Analyst

Accepted Manuscript

This article can be cited before page numbers have been issued, to do this please use: E. Bik, N. Mielniczek, M. Jarosz, J. Denbigh, R. Budzyska, M. Baranska and K. Majzner, *Analyst*, 2019, DOI: 10.1039/C9AN01456J.

View Article Online
DOI: 10.1039/C9AN01456J

ARTICLE

Tunicamycin induced endoplasmatic reticulum changes in endothelial cells investigated *in vitro* by confocal Raman imaging

Received 00th January 20xx,
Accepted 00th January 20xx

DOI: 10.1039/x0xx00000x

Ewelina Bik[a,b], Nikola Mielniczek[a], Magdalena Jarosz[a], Joanna Denbigh[c], Renata Budzynska[b], Malgorzata Baranska[a,b] and Katarzyna Majzner[a,b*]

The paper describes how tunicamycin (Tu), the most widely used pharmacological agents for inducing endoplasmic reticulum (ER)-stress, interacts with endothelial cells. Our results show that tunicamycin enters the cells and accumulates within the ER area. The ER stress takes place when improperly folded or damaged proteins begin to accumulate, however the spectroscopic markers of these changes have not been identified as yet. In this work, Raman spectroscopy and Scanning Electron Microscopy imaging of individual endothelial cells treated with Tu were performed. The changes in biochemical composition of endothelial cells induced by Tu attributed to the ER-stress were studied in detail. A main feature of the Tu impact on cells was a decrease of phospholipids content in the area of ER, and the most abundant lipid with the phosphorus groups found there was identified as sphingomyelin.

Introduction

The endoplasmic reticulum (ER) is a cellular compartment in eukaryotic cells, responsible for the protein folding and for their transport to other parts of a cell or outside[1]. Proteins undergo folding in the ER lumen and are modified by disulphide bonds formation[2,3]. Unfolded proteins are gathered in the ER for a further folding process and degradation, whereas only properly folded proteins are exported to the Golgi apparatus[4]. Perturbations in calcium ion concentration or deregulation of a redox state are the factors, which lead to decreased folding capacity and accumulation of unfolded proteins in the ER lumen[5].A restoration of a balance in the ER, called unfolded protein response (UPR), is maintained by chaperones, which are encoded by gene expression connected with an increased amount of unfolded proteins. The UPR is a cells' way to act in a stressful condition by decreasing protein synthesis, thus lowering the amount of proteins, which enter the ER. The UPR acts also as an increased ER capacity, which enables further processing with unfolded proteins. When the balance between folded and unfolded proteins cannot be restored by these two mechanisms, a cell death is induced. An exposure to stressors can lead to both decrease in the capacity of protein folding and accumulation along with an aggregation of unfolded proteins in the ER lumen. Such phenomena, named as the ER stress, can be evoked by genetic or pharmacological manipulations[6]. The ER stress can lead to inflammatory response[7] and many disorders such as cancer, Alzheimer`s disease, Parkinson disease, diabetes and ischemia are associated with the ER stress[8–15]. Also drug-induced ER stress could lead to several deleterious effects within cells and tissues including accumulation of lipids, apoptosis, cytolysis, and inflammation[16,17]. Tunicamycin (Tu) is one of the most widely used pharmacological agents inducing ER-stress as prototypical toxins in cellular and animal models [18,19]. It has been shown to be an effective inhibitor of the N-glycosylation of many proteins resulting in their improper folding [20,17]. Anticancer properties of Tu were reported [21,22], but the drug was not applied in the cancer treatment because of its toxicity[23,24]. Tu toxic effect was detected *in vitro* on bovine endothelial cells with an evident rough ER dilatation[25]. Tu leads to endothelial cell damage especially in small blood vessels with marked dilatation of the rough ER (i.e., observed also in the presence of ER stress), which in turn distorts their cytoplasm and to cause stenosis of the blood vessel [25,26]. *In vitro* endothelial toxicity has also been observed in vascular endothelial cells by Galan *et al*. [27] and Suganya *et al*. [28]. It has been shown that exposure of endothelial cells to Tu leads to apoptosis through an activation of ER stress. Even *in vivo* studies have showed that ER stress induction leads to a vascular endothelial dysfunction through an oxidative stress generation and p38 MAPK (p38 mitogen-activated protein kinase activity) dependent mechanism, which can be considered as

[a] Faculty of Chemistry, Jagiellonian University, Gronostajowa 2, Krakow, Poland.
[b] Jagiellonian Centre for Experimental Therapeutics (JCET), Jagiellonian University, Krakow, Poland
[c] Biomedical Research Centre, School of Environment and Life Sciences, University of Salford, Salford, United Kingdom

Electronic Supplementary Information (ESI) available: [details of any supplementary information available should be included here]. See DOI: 10.1039/x0xx00000x

intermediates in the impairment of vascular endothelial function by Tu-induced ER stress in a mice model [27].

Raman spectroscopy has been already applied to detect the ER stress in animal cells and tissues[3]. In Raman spectra of cells stimulated with Tu, a decreased intensity of 1443/1453 and 1654 cm^{-1} bands was noticed. allows to assume that these changes are associated with qualitative, quantitative or conformational transformations of the ER proteins[3].

In this work, Raman confocal imaging was used to monitor biochemical changes in single endothelial cells upon stimulation with Tu. This technique has been already successfully applied in order to provide information about biochemical alterations in endothelial cells under various factors[29,30]. The aim of this study however, was to indicate the specific spectroscopic markers of pharmacologically induced ER stress.

Experimental

Materials and methods

Cell culture

Primary human aortic endothelial cells (HAoECs) were selected to study interaction with Tu. A cell line was purchased from Gibco and cultured in the supplemented endothelial cell growth DMEM:F-12 medium (Dulbecco's Modified Eagle Medium/NutrientMixture F-12; ATCC). Cell cultures (passages 2 or 3) were incubated in humidified cell culture incubator (37 °C, 5% CO_2/95% air).

For Raman measurements cells were directly grown on uncoated calcium fluoride windows (CaF_2, 25 × 2 mm, Crystran LTD) placed at a concentration of 180,000 cells per well to obtain appropriate confluence (60-70%). The cells after growth were incubated in a fresh medium for 24 hours in order to achieve their proper adhesion to the surface. Cells were subsequently rinsed twice with phosphate buffered saline (PBS, pH 7.4, Gibco Life Technologies). Afterwards, the cells were exposed to 0.5 and 1 µg/mL of Tu solution (Sigma Aldrich) in DMSO (diluted in the culture medium to obtain final concentrations) for 24 h. After 24 hours of incubation, cells were washed twice with phosphate buffered saline (PBS, Gibco) and fixed for 4 minutes with 2.5% glutaraldehyde. Fixed cells were washed 3 times with PBS and stored in PBS at 4°C until the execution of the measurements.

For Scanning Electron Microscopy (SEM) experiments, HAoECs without and with Tu were seeded on a microscope slide (*c.a.* 0.17 mm thick) for 24 h. Afterwards, the samples were prepared for SEM observations according to the well-established fixing protocol [31,32]. Briefly, samples were fixed with 2.5 % buffered glutaraldehyde for 24 h. Then, they were carefully washed with phosphate buffer solution (PBS) twice for 15 minutes each. Afterwards, they were dehydrated in water-alcohol solutions with increasing ethanol concentration (10 – 100%) for 10 min each. Finally, samples were dried with the use of hexamethyldisilazane (HMDS), twice for 30 s.

Cell viability

For MTT test cells were grown in 96-well plates. After 24h of incubation, with or without Tu, cells were washed 3 times with PBS. To each well 200 µl of media and 20 µl of 0,5 mg/ml 3-(4,5-dimethyl-2-thiazolyl)-2,5-diphenyl-2H-tetrazolium bromide (MTT) were added. Cells were stored for the next 2 h at 37 °C. Afterwards, cells were frozen at -20 °C for 24 h. In the next step defrosted media was removed from the wells. Isopropanol was added to each well and the plate was placed on a plate shaker for 15 min to dissolve a dye. The absorbance of such prepared samples was measured at 562 nm by a Synergy 4 plate reader (Biotek, VT, USA).

Raman measurements

Confocal Raman imaging was applied to track the biochemical composition in the single endothelial cell, as a result of the exposure to Tu. Raman measurement was performed with the use of Confocal Raman Imaging system (WITec alpha 300) supplied with 63× water immersion objective (Zeiss Fluor, NA=1.0), which enables measurements of cells submerged in PBS. The scattered light was directed to the spectrometer *via* 50 µm core diameter multimode fibber, which also acted as the pinhole for the confocal detection. The spectrometer was equipped with UHTS 300 spectrograph and CCD detector (Andor, DU401A-BV-352) and 600 grooves/mm grating (BZL=500 nm). For each measurement, a 532 nm laser was used with a power about 15-20 mW at the sample position. Raman spectroscopic imaging was performed by collecting spectra from cells with 0.5 s exposure time and sampling density of 0.5 µm. For confocal measurements that aimed at imaging the selected cell volume, a higher sampling density (0.120-0.33 µm) was used. The total time of recording a single image ranged between 30÷60 minutes and depended mainly on the size of the imaged area. All spectra were acquired in the 0 – 4000 cm^{-1} spectral range with 3 cm^{-1} spectral resolution.

At least 3 independent biological replicates of each experiment were done and at least 5 cells were measured each time (3 × 5 measurements for each experimental condition were performed). Data acquisition was controlled by WITec alpha 300 software package.

Scanning Electron Microscopy

Fixed samples of cells were mounted on a special holder by using adhesive carbon tape and carbon conductive paint. Finally, in order to provide good conductivity, samples were sputter-coated with a thin layer of gold (approximately 15 nm thick) by using Quorum Q150T S sputter-coater. HAoEC cells were characterized by using a field-emission scanning electron microscope (FE-SEM, Hitachi S-4700) with an accelerating voltage of 20.0 kV.

View Article Online
DOI: 10.1039/C9AN01456J

Data treatment

Pre-processing included cosmic spike removal and background subtraction (with the use of polynomial fit, order 3), were performed using WITec Project Plus Software. Chemical images were generated by using a sum filter. To create Raman images the signal intensity, over a defined wavenumber range representative of the molecular vibrations of interest, was integrated. For data exploration cluster analysis (CA) and Hierarchial Cluster Analysis (HCA) were implemented. The aim of CA is to group analysed objects (spectra) into clusters, hence similar spectra are gathered within the same group. The CA was performed for normalized spectra (normal normalization) with the use of the WITec Project Plus Software (2.10). For *k-means* (KMC) analysis of Raman spectra of the single cells, the distance (object – centroid) was calculated according to the Manhattan (city block) method.

The averaged spectra from classes, acquired from the KMCA, were normalised in the 500-1500 cm^{-1} range, using the OPUS 7.0 software for HCA and PCA analyses. In HCA analysis preceded by spectral normalization, the distance between objects was calculated according to the Euclidean distance. The next step was the analysis of PCA (Principal Component Analysis) carried out in the Unscrambler X software, which was preceded by both standardization (within the ranges 500-1500 cm^{-1} and 2800-3050 cm^{-1}) and smoothing according to Savitzky-Golay method (number of smoothing points was equal to 13).

For selected Raman images a true component analysis was performed (software WITec Project Five).

Results and discussion

In order to study biochemical alterations and structural changes of endothelial cells induced by Tu, two concentrations of this agent were selected. Based on the MTT assay (Fig. 1), Tu at 0.5 and 1 µg/ml was used for the further experiments. These results are in an agreement with several previous reports, where the Tu induced ER-stress was studied using 1-5 µg/mL of this agent[27,28].

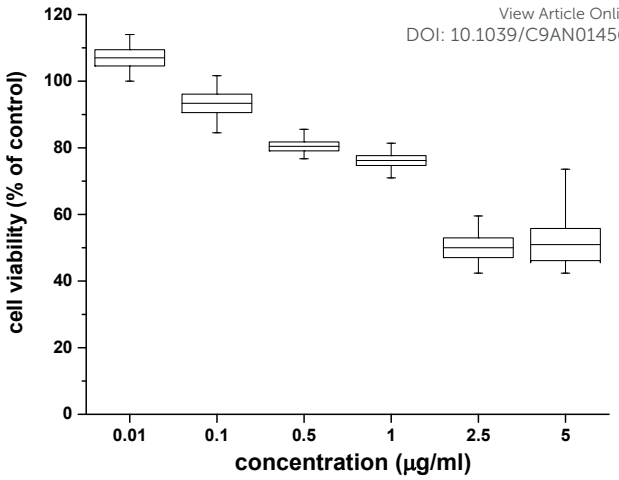

Figure 1 An effect of Tu on HAoECs presented as concentration-dependent reduction of cell viability by Tu treatment for 24 hours. Data are presented as means ± SE (n = 6).

Consequently, in the Figure 2, the representative Raman distribution images of the control cells, and cells stimulated with 0.5 µg/mL and 1 µg/mL of Tu are presented. Two-dimensional Raman images were generated by integrating intensity of characteristic Raman bands of individual cell components, e.g.: organic matter (2830-3030 cm^{-1}, C-H stretching), nucleic acids (775-805 cm^{-1}), lipids (2830-2900 cm^{-1}) and unsaturated lipids (3000-3030 cm^{-1}). Additionally, a distribution of Tu was shown (1050-1200 cm^{-1}). Images of organic matter show the boundaries of cells, whereas integration of bands characteristic for lipids, proteins and DNA helped in identification of cellular organelles.

Raman images were obtained by an integration of the 775-805 cm^{-1} range, covering the 785 cm^{-1} band corresponding to the ring breathing vibrations of the DNA and RNA nitrogen bases, as well as O-P-O skeletal vibrations. They indicate on nucleic acids thus the location of the nucleus in the examined cells. The nucleic acids distribution can be clearly seen only in the image of a control cell (Fig. 2A). Contrary to that, cells stimulated with Tu show characteristic bands at 792 cm^{-1} due to the stimulant (Fig. 3), so by integrating the range of 775-805 cm^{-1} the presence of the nucleus cannot be easily observed (Fig. 2 red and blue panels). Particularly, the Raman image obtained for cells stimulated with 1 µg/mL Tu (Fig. 2, red panel) is considerably different in comparison to the control one, which is dominated by the diagnostic band of DNA (785 cm^{-1}).

View Article Online
DOI: 10.1039/C9AN01456J

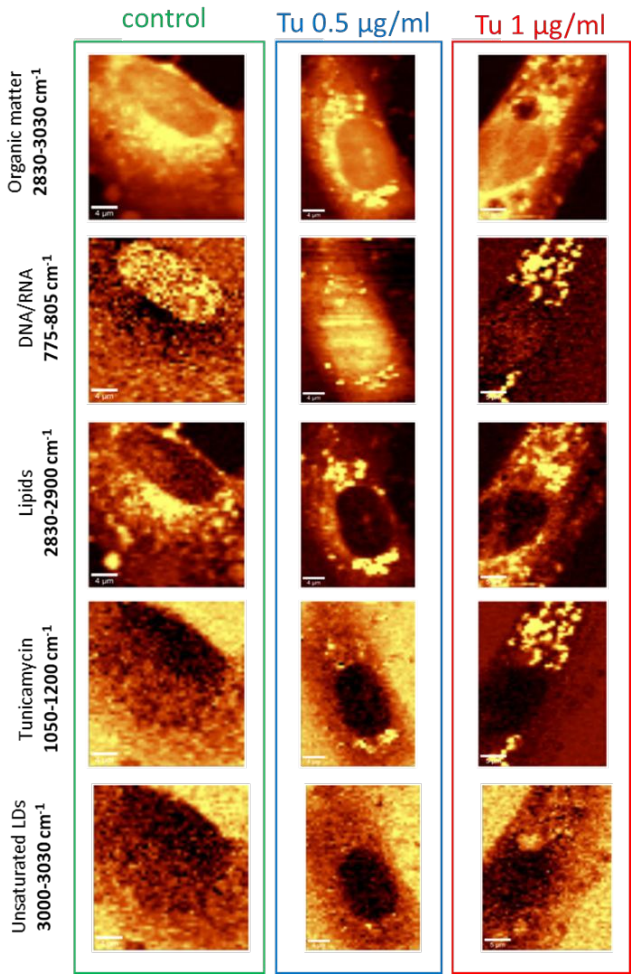

Figure 2 Examples of Raman images of the HaoECs: the control and cells incubated with Tu at 0.5 µg/mL and 1 µg/ml. Integration Raman maps of a specific bands were obtained with 532 nm laser wavelength and with a sampling density of 0.5 µm.

The distribution of lipids can be visualized by an integration of bands within the region of 2830-2900 cm^{-1}. Based on this image it can be seen that cellular lipids partially overlap with the ER. Another image was generated by using bands within the 3000-3030 cm^{-1} range, including the one at 3015 cm^{-1} attributed to stretching vibrations of =CH bond of unsaturated fatty acids. In the presented images (Fig. 2), unsaturated lipid droplets did not occur, however further detailed chemometric analysis revealed small lipidic structures, which can be associated with signal of fatty acids associated with Tu (see structure of Tu in Fig. 3) or can be involved in storage of Tu inside the ER. Czamara *et al.* [33] proposed that unsaturated lipid droplets could reflect the inflammation process of endothelial cells induced by tumor necrosis factor alpha (a cell signaling cytokine involved in systemic inflammation, TNF-α). The absence of unsaturated lipid droplets on the integrated images (Fig.2) allows one to conclude that the ER stress caused by Tu does not follow the mechanism of the cell inflammation[33]. Additionally, the next Raman images were achieved by integration of other characteristic Tu bands within the range 1050-1200 cm^{-1}. This range incorporates the characteristic Tu bands at 1074, 1108 and 1147 cm^{-1} (Fig. 2).

The band at 1073 cm^{-1} in the Tu spectrum (Fig. 3) can be attributed to fatty acids and stretching vibrations originating from C-O bonds in ribose. Moreover, Tu molecule contains sugar moieties that are represented in the Raman spectrum by the presence of the 1111 cm^{-1} band (C-O vibrations). The vibration of C-N group of the uracil molecule can be seen at 1148 cm^{-1}. Additionally, in the spectrum of Tu (Fig. 3) the following intense bands can be noticed: 792 cm^{-1} (breathing mode of the uracil ring), at 1603 cm^{-1} (derived from C = C uracil vibrations) and at 3067 cm^{-1} (stretching vibrations of C-H indicating the presence of aromatic groups). Obtained results strongly suggest that the accumulation of Tu occurs near the nucleus, which corresponds to the location of the ER. Based on that, an accumulation of Tu in the ER area was confirmed.

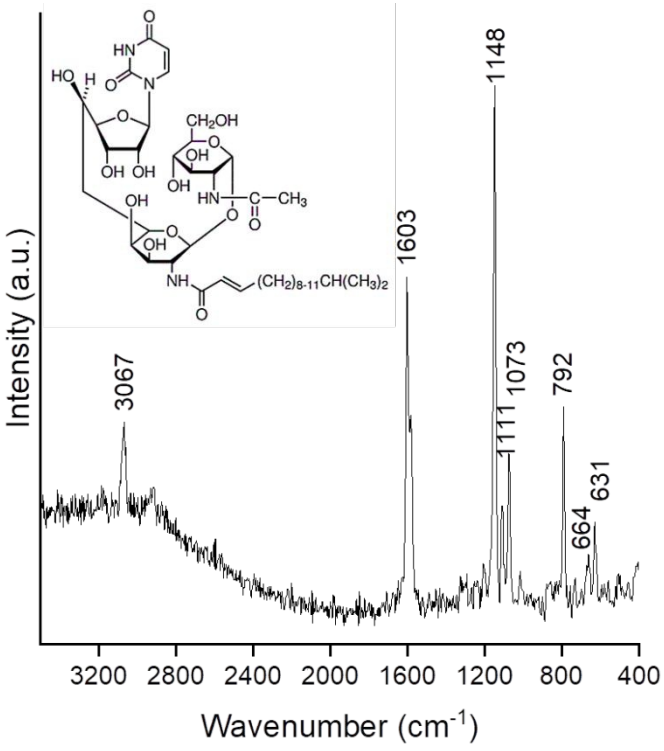

Figure 3. Raman spectrum of Tu (laser excitation wavelength 532 nm) together with its structural formula.

On each spectral data set collected from the cells, the *k*-means cluster analysis (KMC) was performed in order to illustrate cellular components distribution together with the averaged spectra of the individual classes. The KMC analysis enabled visualization of the main compartments of endothelial cells. Representative images of the control cells and Tu exposed HAoECs are presented in the Fig. 4.

View Article Online
DOI: 10.1039/C9AN01456J

ARTICLE

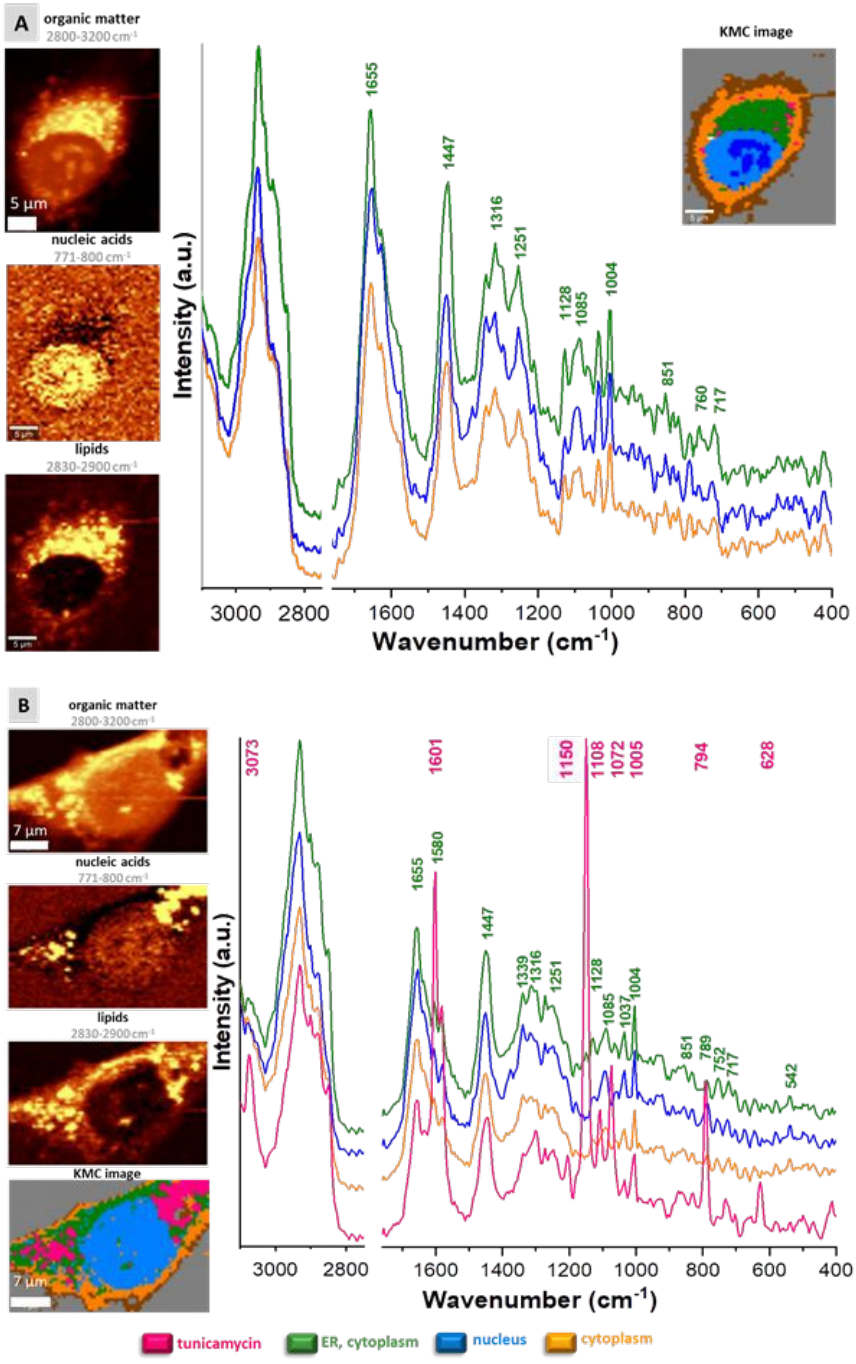

Figure 4. Representative images together with Raman spectra of the main classes for the control HAoECs (A) and cells stimulated with Tu at 1.0 µg / ml (B). Spectra were offset in order to emphasize the differences between them, the Raman intensity in the 2700-3200 cm^{-1} range is 2.5-fold magnified relatively to the fingerprint region. Extracted clusters with the assigned spectra were color coded as follows: nucleoli (dark blue class), nuclei (blue), ER (green), cytoplasm (orange) and cell membrane (brown). An additional class for stimulated cells was distinguished as the one corresponding to the Tu (magenta).

View Article Online
DOI: 10.1039/C9AN01456J

ARTICLE

The class of the ER, which is a membranous structure, was defined and separated based on the 722 cm^{-1} band of the highest intensity in the Raman spectra. It was assigned to the stretching vibrations of the symmetrical $=N(CH_3)_3$ choline moieties associated with phospholipids[34]. This band is observed not only in the ER area but also in the other cell organelles where a phospholipid membrane is separating these organelles from the cytoplasm, and there the band exhibits relatively low intensity. The ER is in charge of the lipids synthesis, which can be confirmed also by the bands within the range 2830-2900 cm^{-1} assigned to lipids, which are of higher intensity in comparison to the spectra collected in any other area of the cell. Furthermore, the cell nucleus was defined based on the characteristic bands at 784, 1096 and 1583 cm^{-1}, corresponding to the vibrations of DNA and RNA. In all classes, bands attributed to proteins can be observed, i.e. 1004 cm^{-1} and 1037 cm^{-1} originating from phenylalanine and at 1255 cm^{-1} and 1661 cm^{-1} assigned to amide III and to amide I, respectively.

Analysis of the ER and lipid rich class in the control and Tu-treated cells indicates an increase of the area, in the case of the latter. The ER cluster, created based on the phospholipids signal, covers larger area around the nucleus, what is especially prominent in the case of 1 µg/mL stimulation. Larger lipids area for Tu-treated cells in comparison to the control can be also observed in the Fig. 2.

The KMC analysis provided details about Tu distribution in the studied cells. Tu is located not only in the area of the reticulum, but also on the periphery of the cell and the cell membrane itself. To confirm the penetration of the compound into the cell, depth profiling was performed (Fig. 5). The results clearly indicate on the presence of Tu inside the cell, especially inside the ER. Fig. 5G shows an overlap of Tu distribution and the ER area (red and magenta class, respectively). Average spectra of both, red and orange spectra, contain Raman features characteristics for the ER area: phospholipids (~720 cm^{-1} and ~ 1086 cm^{-1}) and cytochrome (~750 cm^{-1}) Raman marker bands. The effect of increased volume of the ER due to stress conditions (i.e. misfolded protein aggregates) is known [35,36]. Increased volume and some dilation of ER can be related not only with observed uptake of Tu but also can be related with impaired transport of underglycosylated glycoproteins proteins from rough endoplasmic reticulum to the Golgi complex, such as laminin and fibronectin[37].

To the best of our knowledge, our study is the first one, which reports the enlarged size of the ER that results from the accumulation of Tu. In our opinion, the presence of Tu in the membrane, outside the central area of the cell, can be explained by the electrostatic interaction of the negatively charged membrane with the positively charged Tu. Obtained results suggest that presence of Tu inside the cell is responsible for the ER stress.

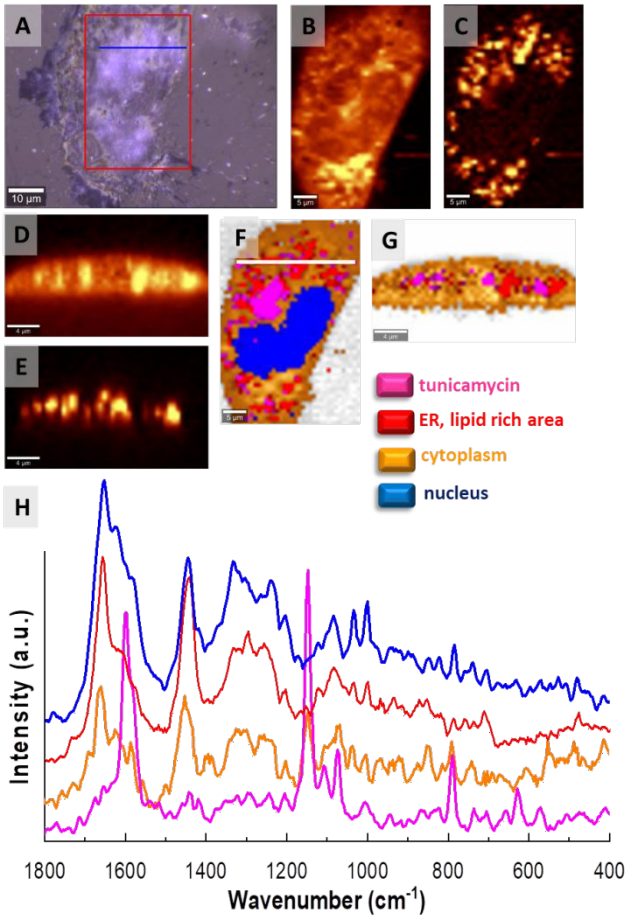

Figure 5. Confocal Raman images of HAoECs exposed to 1 µg/mL of Tu: A – a microphotograph of the cell with marked area for Raman imaging in *x, y* and *x', z,* B,C and D, E – Raman images obtained by the integration of Raman spectra over the selected spectral regions: 3100-2830 cm^{-1} (organic matter), 1565-1615 cm^{-1} (Tu), F and G – true component analysis with main cellular structure with representative spectra of main components in H image.

The next step of analysis was a comparison of the average Raman spectra of the ER region, between control cells and those incubated with Tu (Fig. 6C). As can be seen, averaged spectra of the ER (normalized within the spectral range 500-1500 cm^{-1}), associated with control cells (green) and those from cells stimulated with Tu at a concentration of 0.5 µg / ml and 1 µg / ml (blue and red, respectively) were clearly separated. Averaged spectra of the ER varied mainly in the intensity of three bands at: 785 cm^{-1}

View Article Online
DOI: 10.1039/C9AN01EG1

(associated with vibrations of ring breathing of nucleic bases like uracil, thymine or cytosine [38–40] or O-P-O stretching mode[39,41]), 1089 cm^{-1} (phosphodiester stretching vibrations[40,41]) and 1342 cm^{-1} (adenine, guanine, CH_2 deformation modes[42–44]). For stimulated cells, the intensity of these Raman bands was higher. A position of 1089 cm-1 band can help in biomolecule assignment since a shift to the higher wavenumbers indicates on the presence of nucleic acids[40,45] whereas the shift to lower ones indicates on phospholipids[34,41].

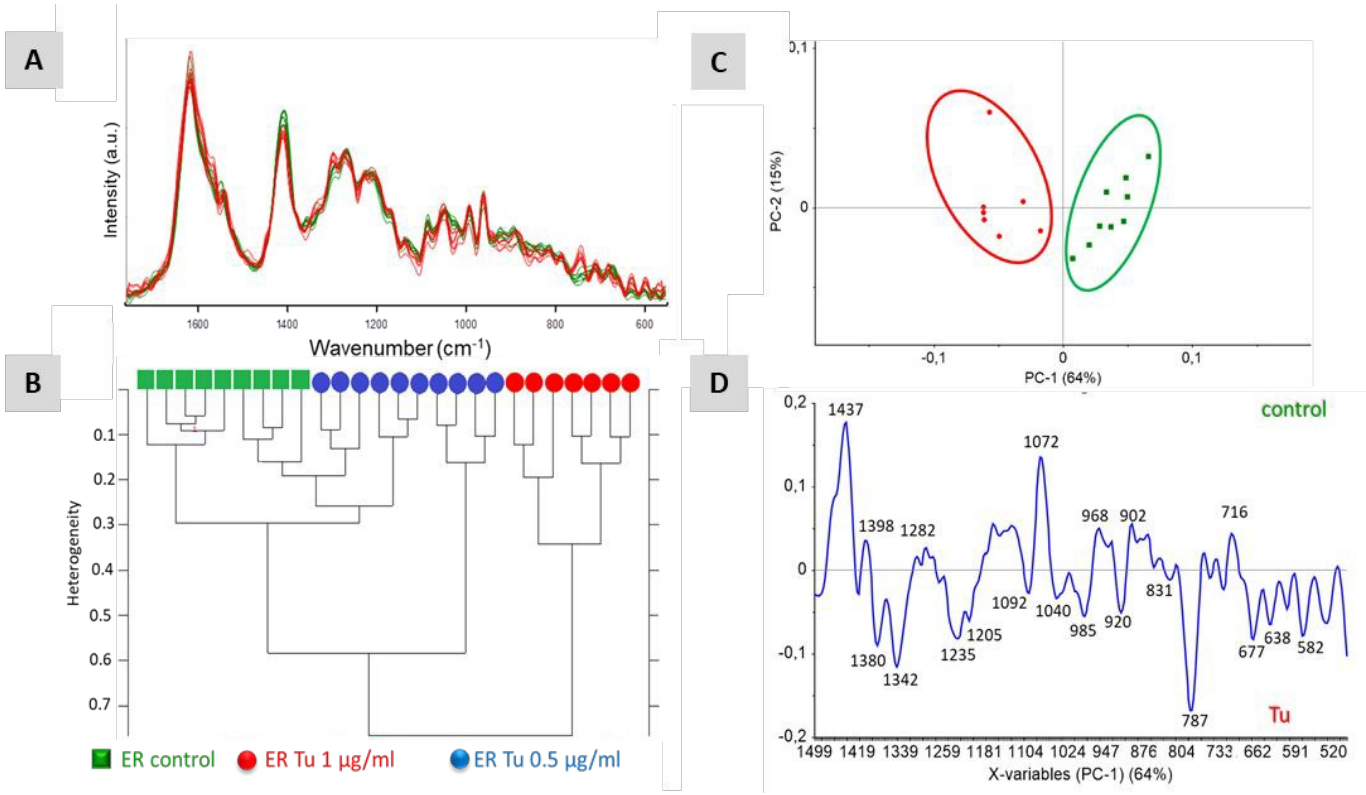

Figure 6. Raman spectra of the ER class extracted from the control (green) and Tu-stimulated HAoECs (A). Hierarchical Cluster Analysis (B) for the control cells (green) and exposed to 0.5 µg/mL (blue) and 1 µg/mL Tu (red). Principal Component Analysis (C) and loadings of the first principal component (D) model for the control cells and exposed to 1 µg/mL Tu. HCA and PCA were done on the vector normalized spectra presented in the panel (A).

In order to check whether the presence of Tu in the ER area affects the biochemical composition of cells, a hierarchical clustering analysis (HCA) was performed. For this approach, the ER spectra obtained as a result of KMCA analysis (coded as a green cluster) were used. Spectra of the ER-rich area of cells presented in Fig. 6A were carefully defined based on relatively high intensity of the 720 cm^{-1} Raman band with no significant Tu Raman features in the spectrum. The HCA was carried out in the following regions: 710-1149, 1197-1298 and 1330-1404 cm^{-1}, which covers the most significant changes in ER spectra between control and Tu-treated cells. Distances between spectra and classification of investigated groups were visualized using the HCA dendrogram. In HCA analysis, spectra were grouped according to their level of similarity. The Fig. 6B shows clearly heterogeneity, especially between the control cells and those stimulated with a higher dose of Tu. The spectra separation obtained using the HCA is at the level of 0.8. A dendrogram of the separation (Fig. 6B) indicates that cells with the higher concentration of Tu differ significantly from the others. In addition, the HCA analysis indicates that the control cells and those stimulated with lower concentration of Tu exhibit some similarities and it is not possible to differentiate them completely during the analysis. This may suggest that at this concentration there are no notable changes in biochemical composition of the ER or alternatively, the amount of Tu is too low and spectra of the ER are not affected by features of Tu. By comparing this result with the MTT viability assay and literature reports, we can assume that low Tu concentration does not promote sufficiently the ER stress or any biochemical changes. On the other hand, the concentration of 2.5 µg/mL of Tu is expected to induce significant changes in endothelial cells. This dose is widely used in pharmacological studies to induce ER-stress in cells, but in our work due to the strong absorbance of the system it was impossible to measure Tu-treated cells. Cells treated with Tu at 2.5 µg/mL or higher concentrations, showed a strong Tu uptake, and were laser sensitive so the photo damaging and burning of the sample was observed. Due to this fact a lower concentrations of Tu were selected.

Principal Component Analysis (PCA) was used to highlight the ER stress markers and to indicate Raman features, which differentiate the control and Tu-treated cells. PCA analysis was performed in the

View Article Online
DOI: 10.1039/C9AN01453J

500-1500 cm^{-1} range. The spectral range was limited to wavenumbers below 1500 cm-1 since bands in 1500-1800 cm^{-1} range can be affected by the O-H bending of water coming from PBS. The most prominent changes were discussed based on the simple analysis of the spectra, but more detailed one with an application of sensitive chemometric tool gives additional information. Results from the HCA were confirmed by the PCA (Fig. 6C). Spectra of the ER from the control cells and cells with a lower dosage (0.5 µg/ml) of Tu were not clearly separated in the HCA. The PCA analysis carried out for the ER spectra of all three groups of cells (control, Tu 0.5 and 1 µg/ml), showed a similar separation to the HCA (Fig. 6B). PCA analysis (Fig. 6C) was conducted for two groups of cells: the control ones (green squares) and stimulated with 1 µg/mL Tu (red triangles). The result of the analysis is a PCA scores and loading plots. In the scatter plot (Fig. 6C) the spectral separation was obtained with respect to the first component (PC-1, reliability row: 64%). Positive values in the loading plot present the bands that characterize control cells versus to the stimulated cells. On the other hand, negative values in the loading plot characterize cells incubated with Tu (Fig. 6D). Detailed analysis of PCA results can help to define spectroscopic markers of ER stress in the cells.

The most significant changes reflected by Raman bands arise from nucleic acids/nucleic bases at 787, 920, 1205, 1235, 1342 cm^{-1}. The intense bands at 1342 and 1380 cm^{-1} are due to guanine vibrations, and the 1380 cm^{-1} band comes from vibrations of both adenine and thymine[46]. In general, the comparison of averaged Raman spectra of the ER area indicates a trend for increased protein signal. The Raman band of phenyloalanine (Phe), which is a good marker of protein signal, is observed on the PCA loading as a shoulder only, what is a consequence of the spectra smoothing. Bands at 1235 and 1342 cm^{-1} can be also assigned to protein (amide III and Trp, respectively)[47] as well as the band at 985 cm^{-1} (Trp)[47], what complicates data analysis.

As mentioned above, Tu-stimulated cells are characterized by a decreased intensity of the band at 715 cm^{-1} corresponding to the stretching vibrations of the choline groups ($N^{+}(CH_3)_3$), and at the 1072 cm^{-1} band attributed to the stretching vibrations of the phosphorous moieties (PO_4^{3-}). Both of these bands are characteristic for phospholipids. Changes in the lipid profile observed in the fingerprint region are in agreement with the one seen in the high wavenumber region (2800-3030 cm^{-1}). Raman bands at 2855 and 2894 cm^{-1} originating from the C-H stretching vibrations of lipids are decreasing in intensity in the Tu-treated cells spectra. This observation can be also made from the PCA analysis (Fig. S1 in Supplementary Material).

Raman results give a proof that Tu, a widely used ER stress inducer, strongly accumulates in the cells and changes chemical composition of lipids in the ER area. Depth profiling measurements showed also the presence of Tu on the cellular surface what suggests it may effect on the membrane. To address the question why Tu is observed not only inside the cells but also outside, the high resolution imaging of the cell surface was performed using SEM. An impact of Tu on morphology of cells or surface of the membrane was previously investigated in the literature by using both the SEM and Transmission Electron Microscope (TEM) [25,37]. Figure 7 shows the representative SEM images of the control and Tu treated cells.

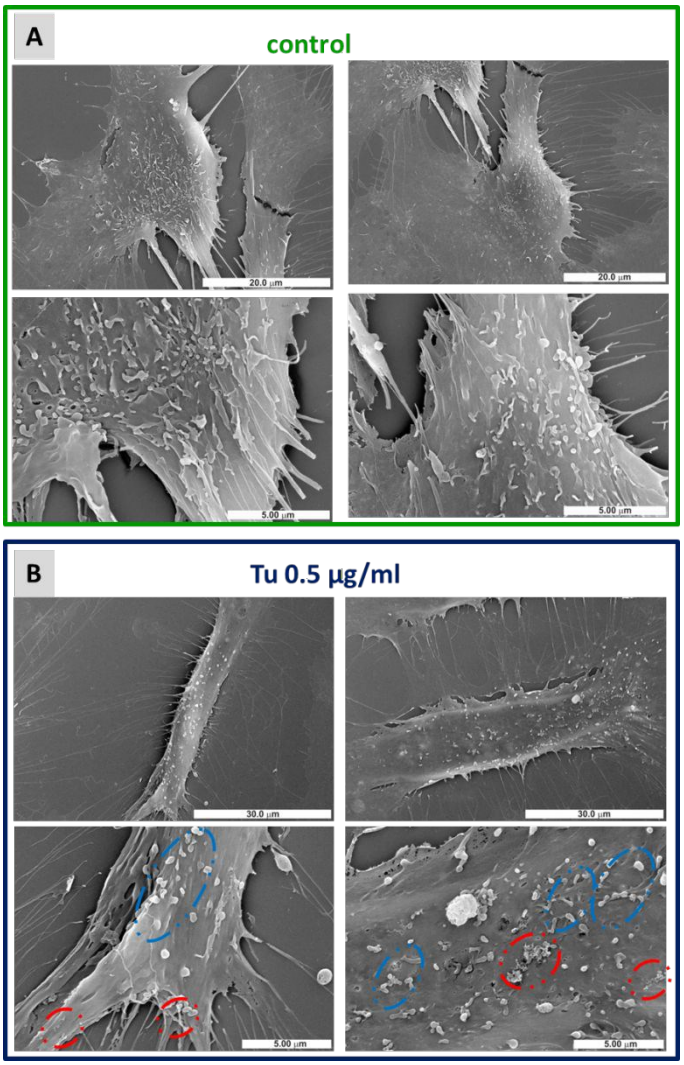

Figure 7 SEM representative images of the control (A) and the cells stimulated with Tu at 0.5 µg / ml (B).

The most prominent changes are marked with red and blue. The main difference between the investigated groups is related to the morphology of microvilli, which cover the membrane and enclose cytoplasm and microfilaments (they can be treated as an extensions from the plasma membrane surface). For the control cells a large number of microvilli on the cellular membrane is observed. Microvilli are elongated objects and after incubation with Tu they are changed and became more globular and knob-like structures (marked with blue arrows in Fig. 7). Microvilli on the surface of endothelial cells act as sensors of changes and if necessary they can activate different intracellular mechanotransduction pathways[48]. Roughness and many perturbations on the cellular surface as a result of Tu interaction were reported before [37]. Results obtained in this work clearly indicate changes in microvilli morphology and

therefore disruptions of their proper functions. Similar membrane protrusions were reported before by using AFM measurements of endothelial cells treated by the TNF-α proinflammatory factor[49]. This type of morphological changes might be an effect of the inflammation process. Moreover, on the surface of Tu-treated cells, the cornflower-like structures are observed (marked in red in the Fig. 7). They are seen mainly at the thinner parts of cell and at the filopodia.

Conclusions

The application of Raman imaging enabled us to study the effect of Tu on endothelial cells. The most significant sign of the Tu impact was enlarged size of the ER that resulted from the accumulation of Tu. Moreover, a decrease of phospholipids content in the area of the ER was observed. Based on the spectra of different phospholipids we can assume that the most abundant lipid occurring there after Tu treatment is sphingomyelin. The increased intensity of bands at 790, 1098, 1206, 1342 and 1380 cm-1 observed in the ER spectra taken from the cells treated with Tu, in respect to the control ones, indicates that the content of nucleic acids is also bigger.

In the situation when the proper functioning of ER is disturbed, its operation is inhibited. Inhibition of a processes in the reticulum also involves the synthesis of lipids, which results in a decrease of fat content in the cell. The inhibition of the new protein synthesis and degradation of unfolded proteins was also observed. Factors activating the initiation of double strand breaks in DNA (DSB) were triggered. All these processes led to an increased amount of nucleic acids and a decrease of phospholipids content.

Results obtained by using SEM clearly indicate changes in morphology of cellular microvilli and therefore disruptions of their proper functions.

Conflicts of interest

There are no conflicts to declare.

Acknowledgements

This work was financed by Ministry of Science and Higher Education (Iuventus Plus, project number 0464/IP1/2016/74) and the National Science Center (UMO-2016/22/M/ST4/00150). The SEM imaging was performed in the Laboratory of Field Emission Scanning Electron Microscopy and Microanalysis at the Institute of Geological Sciences, Jagiellonian University, Poland. EB acknowledges the fellowship with the project no. POWR.03.02.00-00-I013/16. JD acknowledges EU COST action Raman4Clinics. We would like to thank Prof. Stafan Chlopicki for fruitful discussions and helpful advice regarding our data interpretation.

References

1 M. Ogata, S. -i. Hino, A. Saito, K. Morikawa, S. Kondo, S. Kanemoto, T. Murakami, M. Taniguchi, I. Tanii, K. Yoshinaga, S. Shiosaka, J. A. Hammarback, F. Urano and K. Imaizumi, *Mol. Cell. Biol.*, 2006, **26**, 9220–9231.
2 M. Schröder and R. J. Kaufman, *Mutat. Res. - Fundam. Mol. Mech. Mutagen.*, 2005, **569**, 29–63.
3 A. Hosoda, A. Maruyama, D. Oikawa, Y. Oshima, Y. Komachi, G. Kanai, H. Sato and T. Iwawaki, *Biochem. Biophys. Res. Commun.*, 2011, **405**, 37–41.
4 L. Ellgaard, M. Molinari and A. Helenius, *Science*, 1999, **286**, 1882–8.
5 E. Szegezdi, S. E. Logue, A. M. Gorman and A. Samali, *EMBO Rep.*, 2006, **7**, 880–885.
6 D. Ron and P. Walter, *Nat. Rev. Mol. Cell Biol.*, 2007, **8**, 519–529.
7 K. Zhang and R. J. Kaufman, *Nature*, 2008, **454**, 455–462.
8 C. M. Dobson, *Semin. Cell Dev. Biol.*, 2004, **15**, 3–16.
9 S. J. Marciniak and D. Ron, *Physiol. Rev.*, 2006, **86**, 1133–49.
10 H. Yoshida, *FEBS J.*, 2007, **274**, 630–658.
11 L. Pineau, J. Colas, S. Dupont, L. Beney, P. Fleurat-Lessard, J.-M. Berjeaud, T. Bergès and T. Ferreira, *Traffic*, 2009, **10**, 673–90.
12 M. Moenner, O. Pluquet, M. Bouchecareilh and E. Chevet, *Cancer Res.*, 2007, **67**, 10631–10635.
13 M. Kaneko, Y. Okuma and Y. Nomura, 2012, **330**, 325–330.
14 S. Oyadomari and K. Mori, *Artic. Cell Death Differ.*, 2004.
15 U. Ozcan, Q. Cao, E. Yilmaz, A.-H. Lee, N. N. Iwakoshi, E. Ozdelen, G. Tuncman, C. Görgün, L. H. Glimcher and G. S. Hotamisligil, *Science*, 2004, **306**, 457–461.
16 C. Lorz, P. Justo, A. Sanz, D. Subirá, J. Egido and A. Ortiz, *J. Am. Soc. Nephrol.*, 2004, **15**, 380–9.
17 F. Foufelle and B. Fromenty, *Pharmacol. Res. Perspect.*, 2016, **4**, e00211.
18 H. Yoshida, T. Matsui, A. Yamamoto, T. Okada and K. Mori, *Cell*, 2001, **107**, 881–891.
19 F. Urano, X. Wang, A. Bertolotti, Y. Zhang, P. Chung, H. P. Harding and D. Ron, *Science*, 2000, **287**, 664–6.
20 C. Xu, B. Bailly-Maitre and J. C. Reed, *J. Clin. Invest.*, 2005, **115**, 2656–64.
21 Y. H. Jung, E. J. Lim, J. Heo, T. K. Kwon and Y. H. Kim, *Int. J. Oncol.*, 2012, **40**, 1941–1948.
22 J. C. M. de-Freitas-Junior, L. G. Bastos, C. A. Freire-Neto, B. Du Rocher, E. S. F. W. Abdelhay and J. A. Morgado-Díaz, *J. Cell. Biochem.*, 2012, **113**, 2957–2966.
23 D. D. Leaver, K. M. Schneider, M. J. Rand, R. McD. Anderson, P. W. Gage and R. Malbon, *Toxicology*, 1988, **49**, 179–187.
24 C. A. Bourke and M. J. Carrigan, *Aust. Vet. J.*, 1993, **70**, 188–9.
25 J. W. Finnie and J. D. O'Shea, *J. Comp. Pathol.*, 1990, **102**, 363–74.
26 O. J. Finnie JW, *Acta Neuropathol.*, 1988, **74**, 411–21.
27 M. Galán, M. Kassan, P. J. Kadowitz, M. Trebak, S. Belmadani and K. Matrougui, *Biochim. Biophys. Acta - Mol. Cell Res.*, 2014, **1843**, 1063–1075.
28 N. Suganya, E. Bhakkiyalakshmi, S. Suriyanarayanan, R. Paulmurugan and K. M. Ramkumar, *Cell Prolif.*, 2014, **47**, 231–240.

View Article Online
DOI: 10.1039/C9AN01456J

29 K. Majzner, T. Wojcik, E. Szafraniec, M. Lukawska, I. Oszczapowicz, S. Chlopicki and M. Baranska, *Analyst*, 2015, **140**, 2302–2310.
30 T. Wojcik, E. Buczek, K. Majzner, A. Kolodziejczyk, J. Miszczyk, P. Kaczara, W. Kwiatek, M. Baranska, M. Szymonski and S. Chlopicki, *Toxicol. Vitr.*, 2015, **29**, 512–521.
31 W. F. Chissoe and J. J. Skvarla, *Biotech. Histochem.*, 1974, **69**, 192–198.
32 E. R. Fischer, B. T. Hansen, V. Nair, F. H. Hoyt and D. W. Dorward, *Curr. Protoc. Microbiol.*, 2012, **Chapter 2**, Unit 2B.2.
33 K. Czamara, K. Majzner, A. Selmi, M. Baranska, Y. Ozaki and A. Kaczor, *Sci. Rep.*, 2017, **7**, 1–10.
34 K. Czamara, K. Majzner, M. Z. Z. Pacia, K. Kochan, A. Kaczor and M. Baranska, *J. Raman Spectrosc.*, 2015, **46**, 4–20.
35 R. Bravo, V. Parra, D. Gatica, A. E. Rodriguez, N. Torrealba, F. Paredes, Z. V Wang, A. Zorzano, J. a Hill, E. Jaimovich, A. F. G. Quest and S. Lavandero, in *International Review of Cell and Molecular Biology*, 2013, vol. 301, pp. 215–290.
36 J. Mandl, T. Mészáros, G. Bánhegyi and M. Csala, *Mol. Endocrinol.*, 2013, **27**, 384–393.
37 T. Tiganis, D. D. Leaver, K. Ham, A. Friedhuber, P. Stewart and M. Dziadek, *Exp. Cell Res.*, 1992, **198**, 191–200.
38 C. Matthäus, T. Chernenko, J. A. Newmark, C. M. Warner and M. Diem, *Biophys. J.*, 2007, **93**, 668–73.
39 W. L. Peticolas, *Methods Enzymol.*, 1995, **246**, 389–416.
40 B. Prescott, W. Steinmetz and G. J. Thomas, *Biopolymers*, 1984, **23**, 235–256.
41 A. D. Meade, C. Clarke, F. Draux, G. D. Sockalingum, M. Manfait, F. M. Lyng and H. J. Byrne, *Anal. Bioanal. Chem.*, 2010, **396**, 1781–91.
42 I. Notingher, S. Verrier, S. Haque, J. M. Polak and L. L. Hench, *Biopolym. - Biospectroscopy Sect.*, 2003, **72**, 230–240.
43 G. J. Puppels, H. S. Garritsen, G. M. Segers-Nolten, F. F. de Mul and J. Greve, *Biophys. J.*, 1991, **60**, 1046–1056.
44 X. Yiming, Z. Zhixiang, Y. Hongying, X. Yan and Z. Zhiyi, *J. Photochem. Photobiol. B Biol.*, 1999, **52**, 30–34.
45 N. Uzunbajakava, a Lenferink, Y. Kraan, E. Volokhina, G. Vrensen, J. Greve and C. Otto, *Biophys. J.*, 2003, **84**, 3968–81.
46 T. A. Dolenko, S. A. Burikov, E. N. Vervald, A. O. Efitorov, K. A. Laptinskiy, O. E. Sarmanova and S. A. Dolenko, *Laser Phys.*, 2017, **27**, 025203.
47 A. Rygula, K. Majzner, K. M. Marzec, A. Kaczor, M. Pilarczyk and M. Baranska, *J. Raman Spectrosc.*, 2013, **44**, 1061–1076.
48 I. El-Hamamsy, A. H. Chester and M. H. Yacoub, *J. Adv. Res.*, 2010, **1**, 5–12.
49 J. Franz, J. Franz, B. F. Brinkmann, M. König, J. Hüve, C. Stock, K. Ebnet and C. Riethmüller, *PLoS One*, 2016, **11**, e0146598.

View Article Online
DOI: 10.1039/C9AN01456J

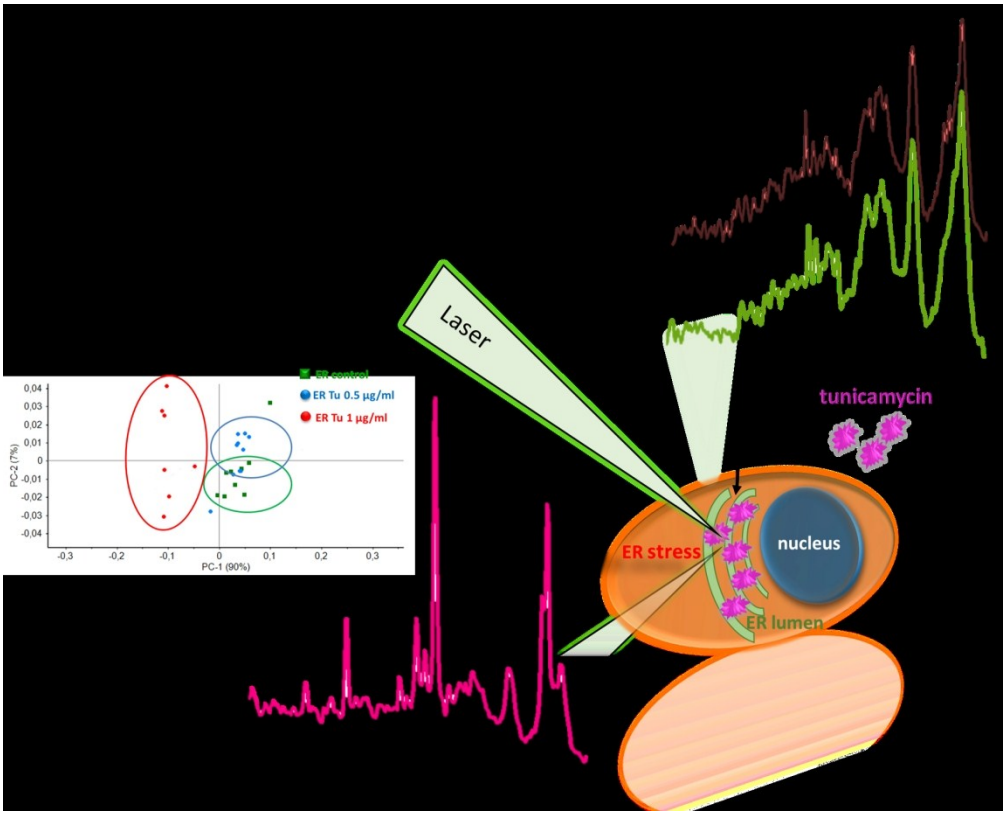

319x257mm (150 x 150 DPI)